Renewable Energy 257 (2026) 124787

Contents lists available at ScienceDirect

Renewable Energy

journal homepage: www.elsevier.com/locate/renene

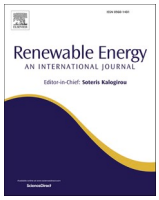

Three-dimensional spatial planning of collection systems in floating offshore wind farms: A two-stage optimization method

Siyu Tao [a,b,*], Jisheng Yang [a], Gang Zheng [c], Andrés E. Feijóo-Lorenzo [d]

[a] College of Automation Engineering, Nanjing University of Aeronautics and Astronautics, Nanjing, 211106, China
[b] Department of Building Environment and Energy Engineering, Hong Kong Polytechnic University, 999077, Hong Kong, China
[c] Monash Biomedical Imaging, Monash University, Clayton, Victoria, 3800, Australia
[d] Department of Electrical Engineering, University of Vigo, Vigo, 36310, Spain

ARTICLE INFO

Keywords:
Floating offshore wind farm
Collection system spatial planning
Dynamic cable
Mooring line movement area
Two-stage optimization

ABSTRACT

The collection system design in floating offshore wind farms (FOWFs) significantly influences both economic viability and operational reliability. This study proposes a two-stage optimization approach to minimize cable costs while ensuring high system performance. In Stage I, floating offshore wind turbines (FOWTs) are grouped using a fuzzy C-means (FCM) clustering algorithm that accounts for both angular separation and spatial proximity. For each resulting cluster, an initial cable layout is generated by constructing a minimum spanning tree (MST) using Prim's algorithm. Stage II applies the Whale Optimization Algorithm (WOA) to refine the routine of dynamic and static cables, optimizing connection points while considering cable parameters and system constraints. In particular, the model ensures that dynamic cables bypass mooring line movement areas (MLMAs) to enhance operational safety. Case studies validate the effectiveness of the proposed method in bypassing MLMAs and reducing overall cable costs. Furthermore, the impacts of loop configurations and seawater depth on cable expenditures are analyzed, providing valuable insights for the planning and design of FOWF collection systems.

1. Introduction

The increasing demand for renewable energy has propelled the development of offshore wind as a vital component of sustainable energy strategies worldwide. The FOWFs have emerged as a promising solution to harness wind resources in deep waters where wind speeds are higher and more consistent, owing to the lower levelized cost of energy (LCOE) of the FOWTs [1,2]. Since the deployment of the world's first MW-scale FOWT in the North Sea in 2009, followed by the commercial operation of the pioneering Hywind project in 2017, the global installed capacity of FOWFs is predicted to reach 31 GW by the end of 2033 [3].

The collection system of an FOWF, which includes the cables and connectors that gather and transmit electricity from individual FOWTs to the offshore substation (OS) is critical to the overall performance and financial viability of the FOWF. As illustrated by Fig. 1, the electricity generated by each FOWT is collected and transmitted through a cable connected to the end of the floating platform. The static section of the cable is buried beneath the seabed while the dynamic section is suspended in seawater using buoy. The movement of the dynamic cable is significantly affected by the motion of the FOWT and by the dynamic loads from the wave and ocean currents. There is a substantial cost difference between dynamic and static cables. Dynamic cables require special materials and reinforced structures to resist more complex and extreme mechanical stresses, with more sophisticated production processes compared to static cables. Cable length is primarily influenced by FOWT spacing, seawater depth, and environmental loads. If the dynamic cable is too long, it results in material waste and increased cost; if too short, it may not withstand the tensile forces caused by FOWT motion, increasing the risk of fracture and restricting the safe motion range of the FOWT. Therefore, optimizing the dynamic cable length is crucial. Additionally, to prevent collisions, dynamic cable routine must bypass MLMAs, making cable trajectory optimization equally important. In this backdrop, the traditional two-dimensional (2-D) static cable layout optimization methods are no longer sufficient. Instead, a three-dimensional (3-D) spatial layout model that balances the project's safety and cost considerations must be developed and applied.

The design and optimization of collection systems for offshore wind farms (OWFs) have been extensively studied, particularly for fixed-bottom installations, which currently dominate the offshore wind energy sector. Stationary offshore wind farms (SOWFs), typically installed

* Corresponding author. College of Automation Engineering, No. 29 Jiangjun Road, Nanjing, 211106, China.
E-mail address: taosiyu@nuaa.edu.cn (S. Tao).

https://doi.org/10.1016/j.renene.2025.124787
Received 24 July 2025; Received in revised form 15 November 2025; Accepted 15 November 2025
Available online 17 November 2025

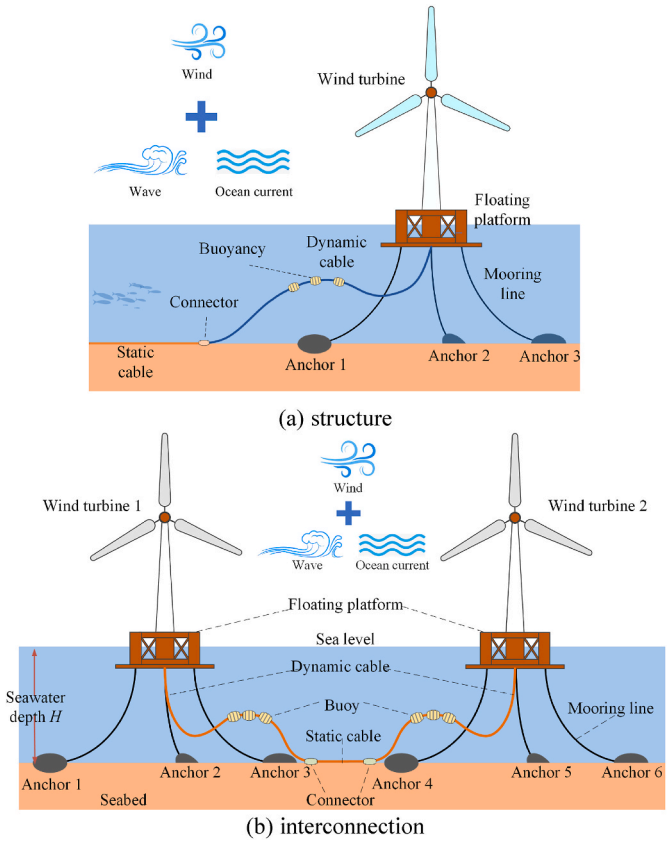

Fig. 1. The FOWT structure and interconnection.

in shallow waters, commonly adopt a well-established 2-D planar planning approach for their collection systems. This approach aims to optimize cable routine while minimizing energy losses [4,5], reducing investment, installation and maintenance costs [6,7], curtailing wind power [8,9] and minimizing environmental impact [10,11], improving revenue [10,12] and system reliability [13,14]. To achieve these objectives, a variety of methodologies have been explored, including heuristic algorithms [15,16], mixed-integer linear programming (MILP) [14,17], mixed-integer quadratic programming (MIQP) [8], double Q-learning (DQL) [11], and graph theory-based approaches [18]. These techniques aim to balance technical feasibility with economic efficiency. For near-shore, shallow-water SOWFs, three typical structures, *i.e.,* the star [19,20], radial [17,21], and ring [8,21] topologies have been widely investigated. Additional efforts have addressed obstacle avoidance [7, 17] and the joint optimization of wind turbine (WT) micro-siting and collection system layout [22]. In planning collection systems for far-shore, deep-sea SOWFs, recent studies have considered wind power curtailment due to wind fluctuation [9] and challenges related to complex seabed topography [21]. Moreover, advanced collection system architectures beyond traditional alternating current (AC) collection system, such as the direct current (DC) series-parallel topology [9], and the DC series-parallel-parallel (SPP) topology [11] have been proposed and optimized.

However, the aforementioned methods are primarily tailored to the static nature of fixed-bottom structures, where seabed conditions and WT positions remain relatively stable. In contrast, research on layout optimization of collection systems for FOWFs is still in its early stages. A design approach for dynamic inter-array cables comprising fatigue analysis and performance assessment in extreme weather conditions were proposed in Ref. [23]. Also, an engineering approach and procedure of designing suspended collector cable configuration for FOWFs was proposed in Ref. [24] with array effects on cable bending radii and tension being investigated [24]. These pioneering studies [23,24] have laid the foundation for FOWF collection system optimization.

Lerch et al. introduced optimization methods using the Particle Swarm Optimization (PSO) algorithm to determine FOWF collector cable layouts [25,26]. While their model separates cables into static and dynamic sections with respective lengths calculation, it assumes that FOWTs are fixed at the platform centers, thereby neglecting the effects of hydrodynamic forces such as wind, wave, and ocean current loads on dynamic cable tension [25,26]. To address economic performance, a techno-economic multi-parametric layout optimization model was developed for an FOWF collection system solved using a gradient-free heuristic optimizer based on a random-search algorithm [27]. Song developed a bi-level optimization model for the FOWF collection systems design. The upper level uses the Binary Particle Swarm Optimization (BPSO) algorithm to optimize the FOWT-OS connections, while the lower level applies the Improved Monte Carlo Tree Search (IMCTS) for determining the inter-FOWT connection [28]. Additionally, Faraggiana investigated the optimization of FOWFs on Mediterranean islands and found that the type of FOWT has a significant impact on the optimal LCOE [29].

Despite these advances, the aforementioned studies overlook a critical constraint: the need to prevent collisions or interference between dynamic cables and mooring lines. The transition from SOWFs to FOWFs represents a paradigm shift in collection system design, necessitating innovative approaches that address the interplay between hydrodynamic forces, cable dynamics, and spatial constraints. While SOWFs benefit from decades of research and practical experience, FOWFs require novel methodologies to ensure efficient power transmission, cost-effectiveness, and long-term reliability. This gap in the literature highlights the need for further research into 3-D spatial planning and optimization techniques tailored to the unique challenges of FOWFs, paving the way for the next generation of offshore wind energy systems.

This study aims to fill the gap by focusing on the 3-D spatial planning and optimization of FOWFs. The innovation lies in enabling cables to bypass MLMAs by optimizing the positions of dynamic-static cable connection points and the mooring angles. The dynamic cable length is optimized according to the movement range of the FOWTs which are installed on semi-submersible platforms. Minimizing the maintenance and replacement costs of cables and additional power losses caused by increased cable failure rates due to collisions between dynamic cables and mooring lines. In Section 2, the mathematical model of the FOWF collection system is formulated; in Section 3, the overall mathematical model along with the solution procedure of the two-stage optimization problem is proposed. Section 4 discusses the simulation results of the case studies and lastly the conclusions are drawn in Section 5.

2. Modeling of the FOWF collection system

2.1. Dynamic cable

As the FOWT has a relatively extensive range of motion, it must be ensured that the dynamic cable can operate safely even when the horizontal distance between the FOWT and its connection joint between the dynamic and the static cables reaches its maximum value. Once the position of the connection joint of the dynamic-static cables and the mooring parameters are determined, the movable range of the FOWT (Fig. 2), the maximum horizontal distance between the joint and the FOWT can be precisely defined. Also, the length of the dynamic cable can be derived. When ensuring that the rectilinear distance from the connection point of the dynamic-static cables to the FOWT does not exceed the maximum allowable distance, a margin ranging from 10 % to 20 % is reserved for the cable length to address installation inaccuracies and extreme scenarios, as expressed by (1).

$$L_{dyn} = (1.1 \sim 1.2)\max\left(\sqrt{H_w^2 + D_{H\,\max}^2}\right) \tag{1}$$

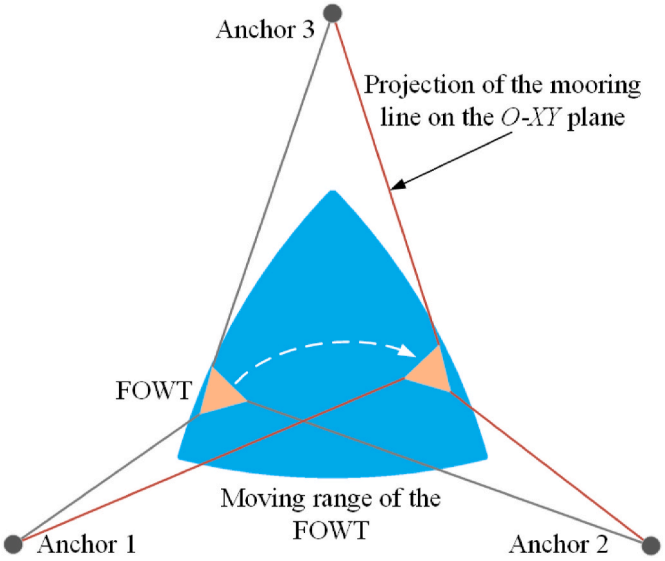

Fig. 2. The FOWT movement range.

where L_{dyn} is the length of the dynamic cable, $H_w = H + \Delta Z$ is the vertical distance between the bottom of the FOWT and the seabed which is not fixed in this context, where H is the seawater depth and ΔZ is the maximum vertical displacement of the floating platform due to waves. $D_{H\,\max}$ is the maximum horizontal distance between the connection joint and the FOWT. As influenced by waves, the FOWT undergoes movement in the vertical direction. Once the mooring parameters are determined, the horizontal movement range of the FOWT changes with the variation of H_w. Thus, it is essential to calculate the cable length by means of the maximum linear distance.

Besides, the dynamic cable also includes buoyancy components and bend stiffeners. The specific quantity of the additional components varies with the length of the cable. Here, only the unit cost of the dynamic cables is roughly considered which is 50 % higher than that of the static cables as given by (2) [29]. The price difference arises from the demanding operational environment of dynamic cables. When applied to the FOWF, they endure constant mechanical stress from waves and currents. To survive these conditions, they require a more robust design including enhanced armoring, greater flexibility, and superior fatigue resistance. These specialized materials and complex manufacturing processes result in a higher unit cost compared to static cables.

$$c_{0\_dyn} = 1.5 c_{0\_stc} \tag{2}$$

where c_{0_dyn} and c_{0_stc} are the prices per unit length of dynamic and static cables, respectively.

2.2. Static cable

The connection between two FOWTs consists of two sections of dynamic cables and one section of static cable. The dynamic cables are directly connected to the FOWTs, and the static cable connects the sections of dynamic cables of two different FOWTs. Assuming that the seabed is flat, the length of the static cable is the Euclidean distance between the two connection heads as calculated by (3).

$$L_{stc} = \|\boldsymbol{L}_{i1} - \boldsymbol{L}_{i2}\|_2 \tag{3}$$

where L_{stc} is the length of the static cable, $\boldsymbol{L}_{i1}$ and $\boldsymbol{L}_{i2}$ represent the coordinates of the two connectors at the end of the i-th static cable, respectively.

3. Two-stage optimization framework

3.1. Optimization model

This paper proposes a two-stage optimization framework. In Stage I, the connection topology between FOWTs is optimized. In Stage II, the connection points and lengths of static-dynamic cables are optimally designed with the goal of bypassing MLMA. The reason for using the two-stage optimization instead of simultaneous optimization of FOWT connections and bypassing MLMA is the dimensionality of optimization variables. Suppose there are N_{wt} FOWTs. Then the optimization problem in Stage I involves connecting N_{wt} nodes. If optimized simultaneously, there will be $2N_{wt}$ nodes including the positions and connections to be optimized. This leads to exponential complexity in cable connections, significantly reducing optimization efficiency, and may even get stuck in an infinite loop without feasible solutions due to cable crossing constraints. Although in Stage II, $2N_{wt}$ nodes are also required to be optimized, the basic topological connections determined in Stage I make the optimization variables relatively independent in Stage II, avoiding exponential complexity. This is the reason why for this optimization problem, the proposed two-stage optimization is far superior to the conventional single-stage optimization.

In Stage I, the FCM algorithm and the MST model are applied to generate the basic topology. In Stage II, the novel WOA [30] is applied, which has gained increasing popularity due to its fewer input parameters, stronger exploration capability, and characteristic of gradually transitioning from global search to fine-grained search. Existing studies have proven that the WOA outperforms the conventional heuristic algorithms [31], *e.g.,* the PSO and the GA.

The two-stage optimization framework of the FOWF collection system planning is illustrated in Fig. 3. In Stage I, the parameters of the FOWF are firstly initialized. An improved FCM based on angle and distance is utilized to cluster the FOWTs. Then, an MST model is established for the FOWTs in each cluster. The topology here merely represents the position of the cables in the horizontal plane, and the distinction between the dynamic and the static cables is not considered in this stage. The topology here only considers linear connections between FOWTs, and only the static cables are used. In Stage II, a group of reasonable mooring angles are calculated according to the cable connections between FOWTs. The mooring angles are configured primarily to bypass MLMAs and minimize cable length as well. Cable segments whose initial linear paths intersect with the MLMAs are assigned offsets. The optimization of the dynamic-static cable connection points ensures the revised path maintains the required separation from the MLMAs. The WOA is used to minimize the total cable cost on the basis of evading the MLMAs, and improvements are made to the specific steps. Finally, the optimal collection system topology, the dynamic-static cable connection points coordinates, cable types and lengths, the mooring angle and the total cable cost are obtained.

3.2. Stage I

1) Model Formulation

The objective of the optimization model in Stage I is to minimize the projection of the collector cables' total length on the *O-XY* plane, L_{cb}^{O-XY} as given in (4). The constraints include the cable type uniqueness constraint, the cable ampacity limitation, the power balance constraint, the topological connectivity constraint, the cable intersection avoidance constraint, and the location constraint of the OS, as sequentially stated in (5).

$$Obj.: \min_{\boldsymbol{z},(x_{os},y_{os},z_{os})} L_{cb}^{O-XY} \tag{4}$$

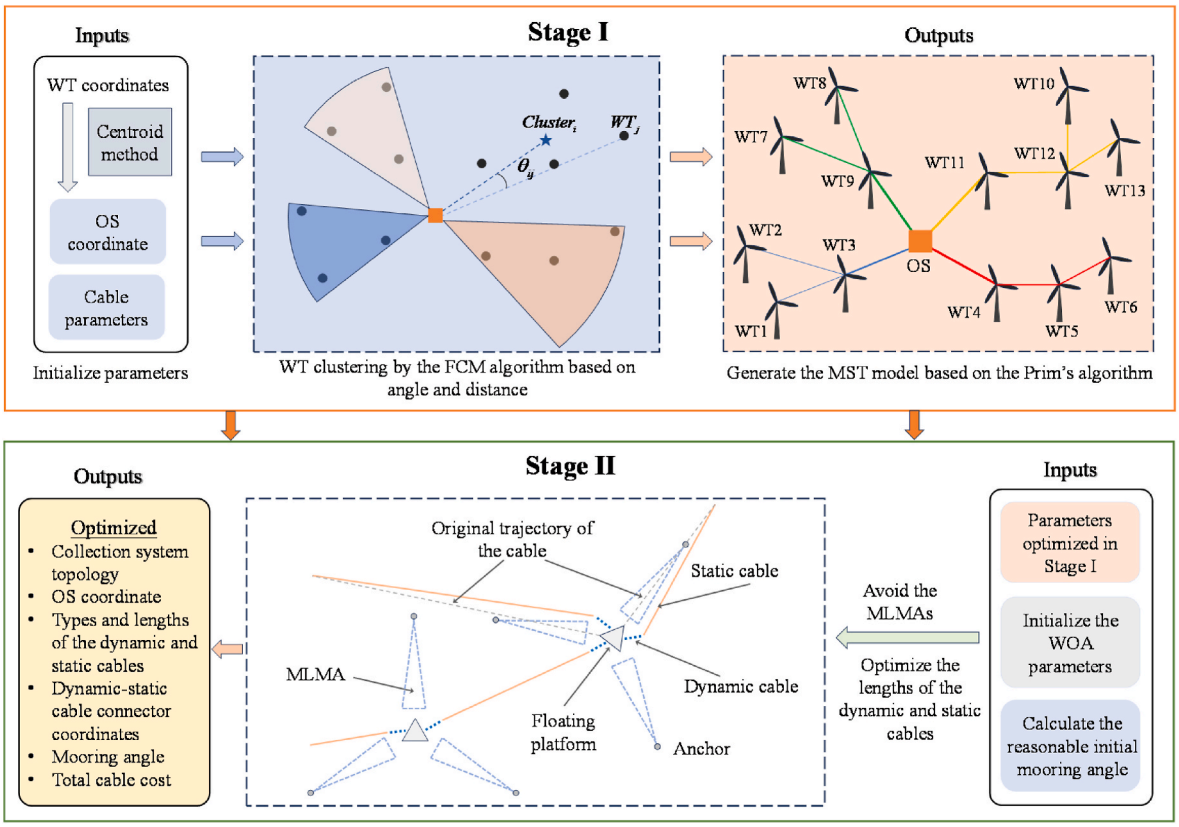

Fig. 3. The two-stage optimization framework.

$$
s.t.\begin{cases}
\sum z_{ijm} \le 1 \\
f_{ij} \le \sum z_{ijm} P_{cb,r,m} \\
\sum f_{ij} = \sum f_{ji} + P_{wt,r} \\
\dfrac{f_{ij}}{P_{wt}} = \sum z_{ijm} + 1 \\
\left(\overrightarrow{AC} \times \overrightarrow{AB}\right) \cdot \left(\overrightarrow{AD} \times \overrightarrow{AB}\right) < 0 \\
\left(\overrightarrow{CB} \times \overrightarrow{CD}\right) \cdot \left(\overrightarrow{CA} \times \overrightarrow{CD}\right) < 0 \\
x_{\min} \le x_{os} \le x_{\max} \\
y_{\min} \le y_{os} \le y_{\max} \\
(x_{os} - X_0)^2 + (y_{os} - Y_0)^2 > l^2 - Z_0^2 \\
8\mathrm{D} \le \sqrt{(X_{0i} - X_{0j})^2 + (Y_{0i} - Y_{0j})^2} \le 12\mathrm{D}
\end{cases} \tag{5}
$$

where the decision variable z_{ijm} indicates the connection status and cable type between the i-th and j-th FOWTs, m indicates the cable type, $m \in \{1, 2, \cdots, M\}$, M is the total number of candidate cable types, the decision variable (x_{os}, y_{os}, z_{os}) is the coordinate of the OS. $P_{cb,r,m}$ is the rated capacity of the m-th type of cable, $P_{wt,r}$ is the rated power of the FOWT, f_{ij} is the power flow on the cable between the i-th and j-th FOWTs. A, B, C and D are the endpoints of two cables, *i.e.*, the FOWTs to be connected (Fig. 4). $[x_{\min}, x_{\max}]$ and $[y_{\min}, y_{max}]$ represent the FOWF boundaries in the x- and y-directions, respectively, $(\boldsymbol{X}_0, \boldsymbol{Y}_0, \boldsymbol{Z}_0)$ are the coordinates of the FOWTs' stationary positions and l is the length of the mooring line. A distance of 8~12 times the rotor diameter D is set between FOWT pairs to avoid aerodynamic interference. (X_{0i}, Y_{0i}) and (X_{0j}, Y_{0j}) represent the stationary coordinate positions of FOWTs i and j, respectively.

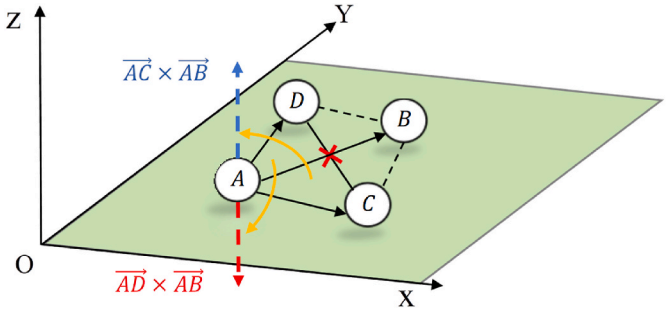

Fig. 4. Illustration of cable intersection avoidance.

2) Solution Procedure

Firstly, the parameters of the FOWF are initialized. Based on the FOWT stationary positions, the centroid of the FOWF is determined. Taking the safe operating distance into account, the location of the OS near the centroid is determined.

The objective of the FCM algorithm based on angle and distance is to minimize the weighted sum of the distances from each FOWT to its respective clustering center, J as given by (6).

$$
J = \sum_{i=1}^{N_{wt}} \sum_{j=1}^{C} u_{ij}^{md} d(\boldsymbol{x}_i, \boldsymbol{c}_j) \tag{6}
$$

where N_{wt} is the total number of FOWTs to be clustered, C is the total number of clusters, $d(\boldsymbol{x}_i, \boldsymbol{c}_j)$ is the weighted comprehensive distance between the azimuth angle difference and the Euclidean distance from each FOWT to its clustering center, $\boldsymbol{c}_j$ is the j-th clustering center, $\boldsymbol{x}_i =$

(x_i, y_i) is the coordinate of the i-th FOWT, u_{ij} represents the membership degree of the i-th FOWT to the j-th clustering center, md is the exponential value of the membership degree matrix whose value is set 2 in this study.

The termination criterion of the FCM algorithm is that the absolute value of the maximum variation of the membership degree u_{ij} between two consecutive iterations is smaller than the error threshold σ, as given by (7).

$$\max\left|u_{ij}^{t} - u_{ij}^{t-1}\right| < \sigma \tag{7}$$

where t represents the number of the iteration being operated, and σ is an extremely small positive number.

To execute the FCM, the C clustering centers are firstly randomly selected, and the comprehensive distance from each FOWT to the clustering centers, d_{ij} can be calculated by (8).

$$d_{ij} = F_j\sqrt{k\cdot\theta_{ij}^2 + (1-k)\left(\frac{\|\boldsymbol{x}_i - \boldsymbol{c}_j\|}{D_{ref}}\right)^2} + \varepsilon \tag{8}$$

where d_{ij} is the distance from the i-th FOWT to the j-th clustering center, F_j is the clustering center correction factor, which is initially set to 1. k is the weighting factor for the angle and the distance which represents the dominance in clustering, *i.e.*, a larger value gives priority to angle, while a smaller value gives it to distance. $\boldsymbol{x}_i$ is the coordinate of the i-th FOWT. D_{ref} is the reference value of the average spacing between the FOWTs. ε is an extremely small positive number to prevent the clustering center coinciding with the position of the FOWT, thus making the comprehensive distance $d_{ij} = 0$. θ_{ij} is the angle difference between the clustering center $\boldsymbol{c}_j$ and the FOWT position $\boldsymbol{x}_i$, which can be calculated by (9).

$$\theta_{ij} = \left|\mathrm{mod}\left(\theta_i - \theta_j, 2\pi\right) - \pi\right| \tag{9}$$

where θ_i is the angle of the i-th FOWT relative to the OS, θ_j is the angle of the j-th clustering center relative to the OS, and "mod" is the modulo function.

Then, the membership degree matrix $\boldsymbol{U}$ with elements u_{ij} can be obtained according to all the comprehensive distances given by (10).

$$u_{ij} = \frac{1}{\sum_{n=1}^{C}\left(\frac{d_{ij}}{d_{in}}\right)^{\frac{2}{m-1}}} \tag{10}$$

where d_{in} is the distance from the i-th FOWT to the n-th clustering center.

The clustering centers are then updated according to (11).

$$\boldsymbol{c}_j = \frac{\sum_{i=1}^{N_{wt}} u_{ij}^m \boldsymbol{x}_i}{\sum_{i=1}^{N_{wt}} u_{ij}^m} \tag{11}$$

A capacity detection of the clusters is conducted through the clustering center correction factor F_j. When the capacity of the FOWTs in a cluster exceeds its upper limit, the value of F_j increases to reduce the membership degree of the FOWTs to the clustering center to achieve the purpose of reducing the capacity as given by (12).

$$F_j^t = F_j^{t-1} + \frac{C_{cluster}}{C_{\max}} \tag{12}$$

where $C_{cluster}$ is the FOWTs capacity in the corresponding cluster, and $C_{\max}$ is the upper limit of the cluster capacity.

The clustering process iterates until the termination criterion in (7) is satisfied. Finally, the Prim's algorithm is applied to solve the MST model in each loop, which is ultimately combined to form the cable topology of the entire FOWF.

3.3. Stage II

1) Model Formulation

The objective of the optimization model in Stage II is to minimize the total cable cost, C_{cb}, constrained by the requirement that cables do not intersect the MLMAs and are within their length limitations, as given in (13) and (14), respectively. The decision variables include the lengths of the static and dynamic cables, L_{stc} and L_{dyn} and the positions of their connectors $(X_{d-s}, Y_{d-s}, Z_{d-s})$.

$$Obj: \min_{L_{stc},\, L_{dyn},(X_{d-s},Y_{d-s},Z_{d-s})} C_{cb} = C_{stc} + C_{dyn} \tag{13}$$

$$s.t.\begin{cases} \overrightarrow{\boldsymbol{L_{dyn}}} \cap S_{moor} = \varnothing \\ \overrightarrow{\boldsymbol{L_{stc}}} \cap S_{moor} = \varnothing \\ L_{dyn,\min} \le L_{dyn} \le L_{dyn,\max} \\ L_{stc,\min} \le L_{stc} \le L_{stc,\max} \end{cases} \tag{14}$$

where C_{stc} and C_{dyn} are the total costs of the dynamic and static cables, respectively, *i.e.*, $C_{stc} = \sum c_{0\_stc,i}\cdot L_{stc,i}$ and $C_{dyn} = \sum c_{0\_dyn,j}\cdot L_{dyn,j}$. S_{moor} is the projection of MLMA on the O-XY plane, $\overrightarrow{\boldsymbol{L_{dyn}}}$ and $\overrightarrow{\boldsymbol{L_{stc}}}$ are the vectors of the dynamic and static cable routines. If one of the ends of the dynamic cable is connected to the FOWT, then $\overrightarrow{\boldsymbol{L_{dyn}}} = (x_{wt}, y_{wt}, z_{wt}) - (X_{d-s}, Y_{d-s}, Z_{d-s})$, where (x_{wt}, y_{wt}, z_{wt}) are the FOWT possible positions which are within its moving rage (Fig. 2); if connected to the OS, then $\overrightarrow{\boldsymbol{L_{dyn}}} = (x_{os},\ y_{os},\ z_{os}) - (X_{d-s},\ Y_{d-s},\ Z_{d-s})$. $\overrightarrow{\boldsymbol{L_{stc}}} = (X_{d-s}, Y_{d-s}, Z_{d-s})_1 - (X_{d-s}, Y_{d-s}, Z_{d-s})_2$ and its length can be obtained from (3). $L_{dyn,\min}$$L_{stc,\min}$, $L_{dyn,\max}$ and $L_{stc,\max}$ are the lower and upper bounds of the dynamic and static cables' lengths, respectively. As illustrated by Fig. 5, according to the minimum and maximum FOWT movement ranges, $L_{dyn,\min}$ and $L_{dyn,\max}$ can be calculated by (15) and (16), respectively. The $L_{stc,\max}$ and $L_{stc,\min}$ are the corresponding static cable lengths in Fig. 5(a) and (b), respectively.

$$L_{dyn,\min} = H_w + \Delta L \tag{15}$$

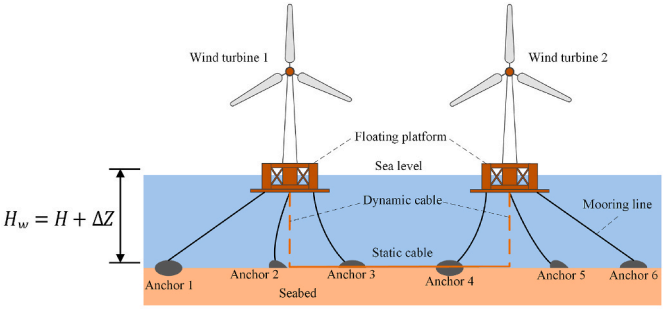

(a) The minimum FOWT movement range.

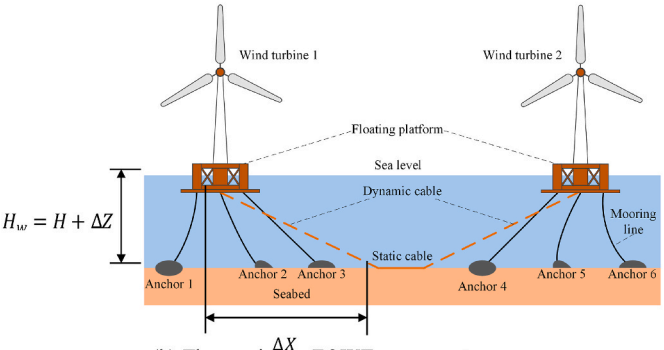

(b) The maximum FOWT movement range.

Fig. 5. Determination of the lower and upper bounds of cable length.

$$L_{dyn,\max} = \sqrt{H_w^2 + \Delta X^2} + \Delta L \tag{16}$$

where ΔL denotes the safety margin length which is 10 %–20 % the total dynamic cable length.

Here, the dynamic cable is of the lazy-wave configuration. If the dynamic cable is too long, the cost will increase significantly; if too short, it may not withstand the stress on the cable, leading to breakage. If the connection head is too close to the stationary position of the FOWT, the curvature of the bent part of the dynamic cable with the buoyancy will be too large, which will significantly impair the mechanism of the cable and shorten its service life. The first two constraints in (14) prevent dynamic and static cables from intersecting MLMAs, thereby ensuring long-term safety for the dynamic cable and reducing installation costs for the static cable. The last two constraints in (14) ensure the optimized lengths of the static and dynamic cables are in their allowable ranges.

2) Solution Procedure

The WOA is employed to solve the optimization model in Stage II. There are two main approaches to optimize cable routine for bypassing MLMA: I) Adjustment of the positions of the two static-dynamic cable connection points between FOWTs to detour cable paths around the MLMA; II) Modification of the mooring angles to eliminate the MLMA-cable intersections which complement each other to achieve the optimum. For ease of initialization and code implementation, the positions of static-dynamic cable connection points are represented as complex numbers. The real part corresponds to the relative *x*-offset, and the imaginary part to the relative *y*-offset, both measured from the dynamic cable's connection point of the FOWT.

The optimization procedure is illustrated in Fig. 6 and its key steps are described in detail as follows.

Step 1: Receive the optimization results of Stage I, that is the stationary position coordinate matrix of the FOWF $WF_{position}$ including the OS coordinate whose node serial number is 1, and the node topology matrix *All_trees* of the MST, $All\_trees \in \boldsymbol{R}^{N_{wt}\times 2}$. Initialize the population size N_{pop} and the maximum number of iterations *MaxIt*.

Step 2: Based on the optimal topology on the *O-XY* plane obtained in Stage I, the reasonable mooring angles are to be optimized for each FOWT's mooring line configuration.

Step 3: Initialize the positional offsets of the dynamic and static cable connectors. The offsets are made to the length and the angle in the direction of the original line as a random initialization. Also, the mooring line angle matrix $\boldsymbol{M}_\Delta$ is randomly initialized by (17).

$$\boldsymbol{M}_\Delta = \boldsymbol{M}_{angle} + \Delta_{angle},\ \Delta_{angle} \in [-30:5:30] \tag{17}$$

where $\boldsymbol{M}_{angle}$ is the most reasonable mooring angle calculated based on the topology determined in Stage I, and Δ_{angle} is the discrete angle for rotating the mooring angle.

Step 4: An individual whale is encoded as $\boldsymbol{X} = [\boldsymbol{Z}_1, \boldsymbol{Z}_2, \boldsymbol{M}_\Delta]$, where $\boldsymbol{Z}_1$ and $\boldsymbol{Z}_2$ correspond to the positional offsets of the dynamic-static cable connection points relative to the nodes in the first and second columns of *All_trees*, respectively, $\boldsymbol{M}_\Delta$ is the mooring angle matrix of the N_{wt} FOWTs, $\boldsymbol{Z}_1, \boldsymbol{Z}_2, \boldsymbol{M}_\Delta \in \boldsymbol{R}^{N_{wt}\times 1}$, where $\boldsymbol{R}$ represents the set of real numbers. To realize bypassing MLMA, the objective function incorporates penalties based on the number of cable-MLMA intersections. A cable routine consists of two dynamic cable segments and one static cable segment, all need to be checked for intersections with the MLMA. This study uses an intersection degree matrix, $\boldsymbol{X}$.cross to measure the number of cable-MLMA intersections, with the same dimension as $\boldsymbol{X}$. The first and second columns of $\boldsymbol{X}$ indicate whether the corresponding dynamic cables intersect with MLMA, while the third column of $\boldsymbol{X}$ denotes whether the dynamic cables connected to FOWTs and the adjacent static cables intersect with the MLMA, where 1 represents an intersection while 0 no.

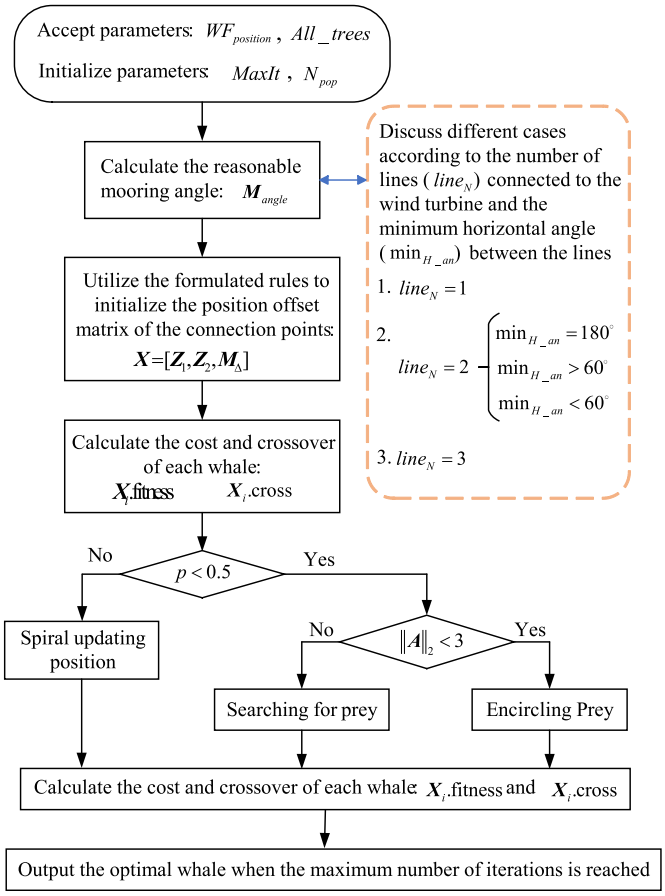

Fig. 6. Solution procedure of the Stage II optimization model.

Step 5: Calculate the intersection degree matrix, $\boldsymbol{X}$.cross based on the information of whales, and simultaneously compute the fitness function, $\boldsymbol{X}$.fitness as given in (18).

$$\boldsymbol{X}.\text{fitness} = (1 + \text{sum}(\boldsymbol{X}.\text{cross}))^2 \cdot C_{cb} \tag{18}$$

The fitness value is amplified based on the number of cable-MLMA intersections and it equals the total cable cost only if the cable routine contains no MLMA intersections.

Step 6: After the initialization of the first generation of the whale population, the update path is selected based on the random number p within the range of $p \in [0,1]$.

When $p < 0.5$, the whales' positions are updated via the spiral equation in (19).

$$\boldsymbol{X}(t+1) = \boldsymbol{D} \cdot e^{b\cdot r} \cdot \cos(2\pi \cdot r) + \boldsymbol{X}_{best}(t) \tag{19}$$

where $\boldsymbol{D} = |\boldsymbol{X}_{best}(t) - \boldsymbol{X}(t)|$ is the distance between the current optimal solution and the current search agent, b is a constant defining the spiral shape (typically set to 1), and r is a random number within the range of $[-1,1]$. t represents the iteration number.

When $p \geq 0.5$, the whales' positions update following two modes based on the 2-norm of the coefficient vector $\boldsymbol{A}$. When $\|\boldsymbol{A}\|_2 < 3$, whales search for prey according to (20).

$$\boldsymbol{X}(t+1) = \boldsymbol{X}_{rand}(t) - \boldsymbol{A} \cdot |\boldsymbol{C}\boldsymbol{X}_{rand}(t) - \boldsymbol{X}(t)| \tag{20}$$

where $\boldsymbol{A} = 2a\cdot\boldsymbol{r} - a$ and $\boldsymbol{C} = 2\cdot\boldsymbol{r}$ are the two coefficient vectors, a is a parameter that linearly decreases from 2 to 0 during iterations, and $\boldsymbol{r}$ is a

random matrix whose elements are within the range of $[0,1]$. Both $\boldsymbol{A}$ and $\boldsymbol{C}$ are matrices with dimensions consistent with $\boldsymbol{X}$. This matrix operation utilizes the Hadamard product, *i.e.*, an element-wise multiplication operation. $\boldsymbol{X}_{rand}(t)$ is a randomly selected whale individual in the t-th generation.

When $\|\boldsymbol{A}\|_2 \geq 3$, whales encircle the prey and update their positions according to (21).

$$\boldsymbol{X}(t+1) = \boldsymbol{X}_{best} - \boldsymbol{A} \cdot |\boldsymbol{C}\boldsymbol{X}_{best} - \boldsymbol{X}(t)| \tag{21}$$

where $\boldsymbol{X}_{best}$ denotes the current optimal individual with the minimum fitness value.

After updating the positions of the whale population, calculate the intersection degree matrix, $\boldsymbol{X}$.cross and fitness function, $\boldsymbol{X}$.fitness for all the whale individuals.

Step 7: Repeat the position update and fitness function calculation in **Step 6** iteratively until the number of iterations reaches *MaxIt*. Then, output the optimal whale individual.

4. Case study

4.1. Test system

In this paper, an FOWF in Golfe de Fos installed with 36 DTU-10 MW FOWTs along with the OO-Star semi-submersible platform is set as the test system [32]. The distance between the FOWTs is 8 times their rotor diameter for safety consideration. The specific parameters for simulation are given in Table 1 [32,33].

The FOWF to be planned adopts a 66 kV collection system [26] and the cable parameters are shown in Table 2.

4.2. Results and discussion

Stage I is firstly carried out in which only the projection of the cables on the *O-XY* plane is considered. The clustering results have a decisive influence on the generated power collection topology. There are two key parameters involved, *i.e.*, the number of clusters, C whose values are from 6 to 9 with steps of 1, and the weighting factor of the distance and angle, k whose values are from 0.1 to 0.9 with steps of 0.05. When the cluster number is determined, the clustering degree is decided by k. Thus, multiple values of k are tested to identify the minimal-cost collection system topology of the FOWF under a specified cluster. The corresponding collection system topologies with the best fitnesses are generated respectively of different numbers of clusters.

Then, the basic topologies obtained from Stage I are separately transferred to Stage II. The optimized total costs of the dynamic and static cables are given in Table 3 where $C_{cb,opt}$ is the optimal FOWF collector cable cost, $C_{dyn,opt}$ and $C_{stc,opt}$ are the costs of dynamic and static cables optimized in Stage II, respectively. It can be observed that the changing trends of the cable costs in the two stages with different basic topologies are the same. This demonstrates that the basic topology is the main factor determining the cable cost. Also, for FOWF collection systems employing both dynamic and static cables, static cables constitute the predominant portion of total cable length, making this cost dominance self-evident.

The comparison of the optimal cable lengths after two-stage optimization of the aforementioned cluster numbers ($C = 6, 7, 8, 9$) are shown in Fig. 7. Among them, the ratio of the optimal length of the dynamic cable, $L_{dyn,opt}$ to that of the static cable, $L_{stc,opt}$ is approximately between 0.3 and 0.4.

It can be seen from Fig. 7 that the optimal total length of the dynamic cables decreases as the number of clusters increases, which is opposite to the changing trend of the static cables. However, for the topological structures with smaller number of clusters, power flows are higher in the cables close to the OS in the FOWF, and their corresponding optimal total cable costs are also higher. Therefore, the total length of the cables in the FOWF collection system with 6 clusters is the shortest, but its optimal total cable cost is the highest, with the value of $C_{cb,opt} = 22.095$ M€. Therefore, compared with cable length, the power capacity of the cable has a greater impact on the total cost in the FOWF collection system. As can be seen from Table 3, the optimal total cable cost $C_{cb,opt}$ is the lowest when the number of clusters C is the largest, $C_{\max} = 9$.

The projection of the optimal FOWF collection system topology on the *O-XY* plane obtained from Stage I is shown in Fig. 8. It can be seen that the FOWTs are partitioned into 9 groups each containing 3 to 6 FOWTs. However, this schematic only demonstrates basic 2-D planar connection relationship between FOWTs and between FOWTs and OS. The lengths and the detail routine of the dynamic and static cables in 3-D space are to be optimized in Stage II on the basis of the optimal topology in Fig. 8.

The optimal FOWF collection system topology that bypasses the MLMAs obtained from Stage II is shown in Fig. 9.

Fig. 9 shows that even after optimizing mooring angles, some cables may still intersect MLMAs. For these cases, a direct straight-line connection between dynamic and static cable segments is infeasible.

Table 1
Simulation parameters.

FOWT rotor diameter (m)	Seawater depth (m)	Maximum wave amplitude (m)	Mooring line length (m)
178	70	7.5	380

Table 2
The 66 kV collector cable parameters.

Cross section (mm^2)	95	150	300	400	630	800
Power capacity (MW)	23	30	40	50	63	71
c_{0_stc} (€/m)	219	300	423	474	554	689
c_{0_dyn} (€/m)	328.5	450	634.5	711	831	1033.5

Table 3
Optimized cable costs of different cluster numbers.

Number of clusters, C	6	7	8	9
$C_{cb,opt}$ (M€)	22.095	21.4404	21.0734	20.3013
$C_{stc,opt}$ (M€)	14.4535	14.278	14.2471	14.0721
$C_{dyn,opt}$ (M€)	7.6415	7.1624	6.8262	6.2292

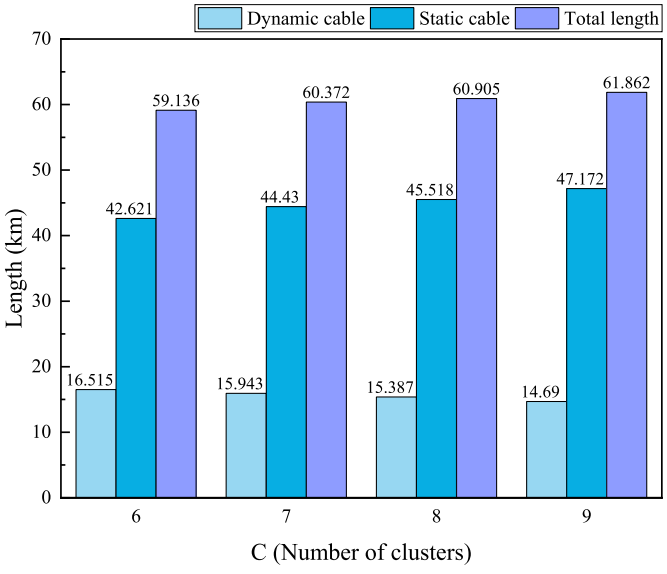

Fig. 7. Cable length of the FOWF collection system.

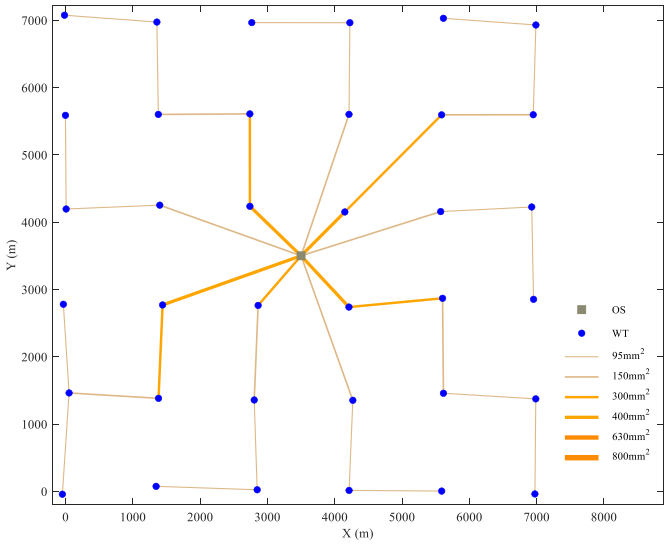

Fig. 8. Projection of the optimal FOWF collection system topology on the *O-XY* plane obtained from Stage I.

Relocating cable connection points to bypass MLMAs marginally increases dynamic cable costs but can significantly reduce mooring line-cable collisions during FOWT motion, extending cable service life. This repositioning also lowers dynamic cable installation complexity and cost. In Table 3, although the cable costs generally decrease with loop number, the 10-loop has higher costs (20.5173 M€) than the 9-loop topology. This means that maximizing loops cannot guarantee cost minimization. As loop number rises, cable length grows disproportionately, making length-driven costs dominate over power capacity savings. Furthermore, excessive loops force export cables near the OS closer together. This proximity sharply increases MLMA avoidance complexity and cost, sometimes making avoidance infeasible. Therefore, an optimal loop number exists for FOWF collection topology optimization.

The simulation of a comparative case is carried out where cable topology optimization excludes MLMA avoidance and the mooring angles remain fixed at their initial configurations and the optimal FOWF collection system layout is given in Fig. 10, with a total cable cost of 20.6202 M€, slightly higher than the 20.3013 M€ of the two-stage optimization. This means that optimizing the positions of dynamic-static cable connection points results in the cables not being the shortest straight lines in the horizontal plane, but it is necessary that the dynamic cables must accommodate the maximum movement distance of FOWTs.

Therefore, when the FOWT movement areas are completely identical, directional imbalances of cable lengths may incur, that is to say, the dynamic cables in certain directions may be forced to be exceptionally long which will lead to higher costs. From simultaneous optimization of mooring angles and connection points in Stage II, cable routine can bypass MLMAs while mitigating cost escalation.

As can be observed in Fig. 10, the MLMA intersections occur with 25 dynamic cable segments and 13 static cable segments which pose critical risks. For dynamic cables, such intersections will induce potential collisions with the mooring lines which will degrade their service life and increase failure probability, resulting in high replacement costs and significant power losses from cable failures. Intersections between static cables and MLMA also substantially increase the installation costs of the crossed cable sections. This validates that the inclusion of the MLMA avoidance into the FOWF collection system planning is essential for its operational efficiency and cost reduction.

To analyze the influence of seawater depth on the optimization results of the proposed model, four different seawater depth values are tested ($H = 70$ m, 90 m, 110 m, 130 m). Adjusting the mooring parameters for different water depths, and the results are given in Table 4 and Fig. 11.

The simulation results in Table 4 indicate that dynamic cable length grows substantially with seawater depth, while static cable length remains relatively stable. It means that the dynamic cables are the primary contributor to total cost growth.

Besides, the cost comparison of different seawater depth groups in Fig. 11 reveal decreasing marginal costs for dynamic cables with the increase of seawater depth. This is because the mathematical relationship between the length increment of the dynamic cable and the seawater depth increment approximately follows a negative quadratic relationship, and the increment ratio gradually decreases.

5. Conclusions

This paper proposes a two-stage optimization model for the planning of the collection system of a FOWF. The model successfully minimizes the total cable cost while ensuring dynamic cables bypassing MLMAs, thereby enhancing the safety of the FOWF collection system. Case studies yield the following findings.

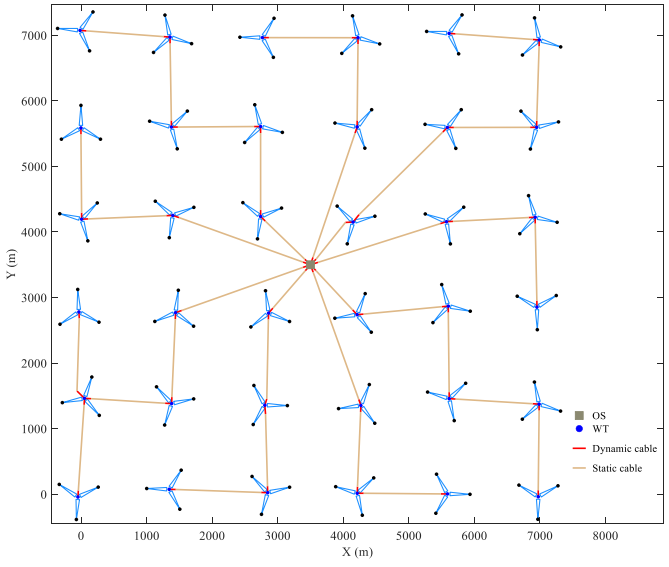

Fig. 9. Optimal FOWF collection system topology that bypasses the MLMAs obtained from Stage II.

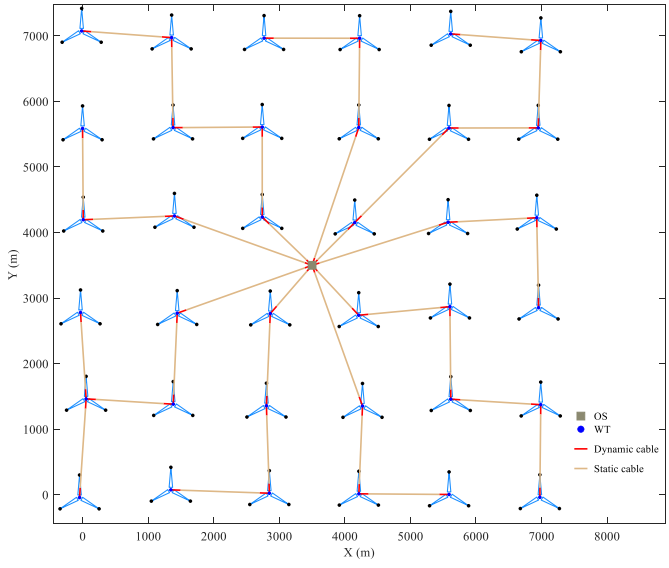

Fig. 10. Optimal FOWF collection system topology without MLMA avoidance.

Table 4
Optimization results of different seawater depths.

Seawater depth H (m)	70	90	110	130
$C_{cb,opt}$ (M€)	20.3013	21.289	22.1088	22.9226
$C_{stc,opt}$ (M€)	14.0721	14.0934	14.1199	14.1441
$C_{dyn,opt}$ (M€)	6.2292	7.1956	7.9889	8.7785
$L_{cb,opt}$ (km)	61.862	64.164	66.128	68.086
$L_{stc,opt}$ (km)	47.172	47.223	47.307	47.396
$L_{dyn,opt}$ (km)	14.69	16.941	18.821	20.69

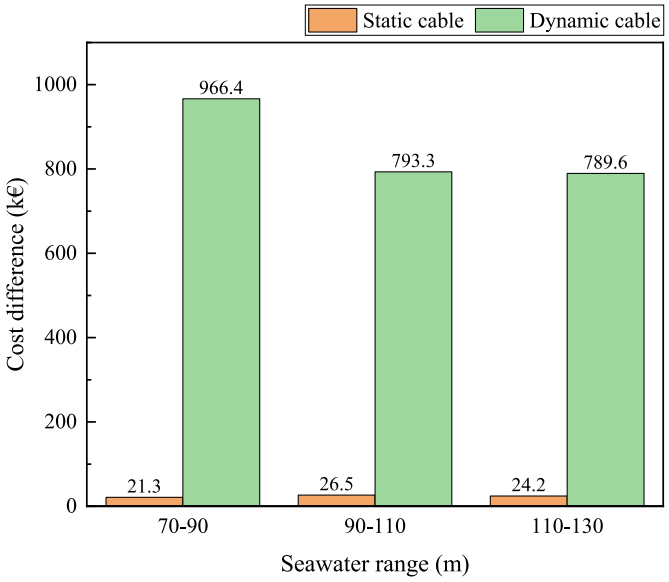

Fig. 11. Cost differences under different seawater ranges.

1) In Stage I, the FCM clustering method based on angles and distances has a remarkable effect on the optimization of the collection system topology of the FOWF with OS located inside.
2) When partitioning and grouping FOWTs, there exists an optimal number of clusters in Stage I for which the cable length and the power capacity can achieve the best balance.
3) In Stage II, increased seawater depth significantly raises dynamic cable costs in the FOWF, though the marginal cost increase diminishes with greater depth.
4) In Stage II, routing dynamic and static cables to bypass MLMAs significantly reduces potential collisions with mooring lines, extending cables' service life, lowering installation difficulty and cost.

Future work will prioritize cable optimization to minimize the LCOE of the FOWF, integrating FOWT micro-siting into cable configuration design. Particular attention will be paid to analysis of power fluctuations from FOWT movement, topological power losses, and the economic impacts of cable damage to establish a robust optimization framework.

CRediT authorship contribution statement

Siyu Tao: Writing – review & editing, Writing – original draft, Supervision, Resources, Project administration, Methodology, Investigation, Formal analysis, Data curation, Conceptualization. **Jisheng Yang:** Writing – original draft, Visualization, Validation, Software, Methodology, Data curation, Conceptualization. **Gang Zheng:** Writing – review & editing. **Andrés E. Feijóo-Lorenzo:** Writing – review & editing.

Data availability statement

The data that support the findings of this study are available from the corresponding author upon reasonable request.

Funding information

This work was supported in part by the National Natural Science Foundation of China under Grant 52207111 and 52577112, the Hong Kong Scholars Program under Grant XJ2024024, the Open Fund of State Key Laboratory of Power System Operation and Control under Grant SKLD24KM18, the Open Fund of State Key Laboratory of Ocean Engineering under Grant 2449, the Open Fund of State Key Laboratory of Alternate Electrical Power System with Renewable Energy Sources under Grant LAPS25013, the Open Fund of Jiangsu Key Laboratory of Power Transmission & Distribution Equipment Technology under Grant 2025JSSPD01, and the Jiangsu Province Science and Technology Think Tank Youth Project under Grant JSKX0125080.

Declaration of competing interest

The authors declare that they have no known competing financial interests or personal relationships that could have appeared to influence the work reported in this paper.

References

[1] S. Tao, J. Yang, G. Zheng, et al., A two-stage optimization model for floating offshore wind farm layout and control, Renew. Energy 253 (2025) 18, https://doi.org/10.1016/j.renene.2025.123614.
[2] Z. Liang, H. Liu, Novel yaw-based wake modelling and controlling to enhance the power output of floating offshore wind farms, Renew. Energy 256 (2025) 14, https://doi.org/10.1016/j.renene.2025.123838.
[3] Global Wind Energy Council, Global offshore wind report [online]. Available: https://www.apren.pt/contents/publicationsothers/gwec-gowr-2024-digital-final-2-compressed-1.pdf, , 2024.
[4] J. Pérez-Rúa, S. Lumbreras, A. Ramos, et al., Reliability-based topology optimization for offshore wind farm collection system, Wind Energy 25 (1) (2022) 52–70, https://doi.org/10.1002/we.2660.
[5] Z. Huang, C. Yuan, H. Ge, et al., Optimization of substation siting and connection topology in offshore wind farm based on modified firefly Algorithm, IEEE Journal on Emerging and Selected Topics in Circuits and Systems 13 (3) (2023) 806–816, https://doi.org/10.1109/jetcas.2023.3290161.
[6] J. Pérez-Rúa, M. Stolpe, K. Das, et al., Global optimization of offshore wind farm collection systems, IEEE Trans. Power Syst. 35 (3) (2020) 2256–2267, https://doi.org/10.1109/tpwrs.2019.2957312.
[7] J. Pérez-Rúa, M. Stolpe, N. Cutululis, Integrated global optimization model for electrical cables in offshore wind farms, IEEE Trans. Sustain. Energy 11 (3) (2020) 1965–1974, https://doi.org/10.1109/tste.2019.2948118.
[8] X. Shen, Q. Wu, H. Zhang, et al., Optimal planning for electrical collector System of offshore wind farm with double-sided ring topology, IEEE Trans. Sustain. Energy 14 (3) (2023) 1624–1633, https://doi.org/10.1109/tste.2023.3241357.
[9] Y. Fu, Y. Liu, L. Huang, et al., Collection System topology for deep-sea offshore wind farms considering wind characteristics, IEEE Trans. Energy Convers. 37 (1) (2022) 631–642, https://doi.org/10.1109/tec.2021.3104040.
[10] S. Wei, H. Wang, Y. Fu, et al., Electrical System planning of large-scale offshore wind farm based on N+ design considering optimization of upper power limits of wind turbines, Journal of Modern Power Systems and Clean Energy 11 (6) (2023) 1784–1794, https://doi.org/10.35833/mpce.2022.000656.
[11] C. Pan, S. Wen, M. Zhu, et al., DC Collector System layout optimization for offshore wind farm with SPP topology, IEEE Trans. Sustain. Energy 16 (2) (2025) 1269–1282, https://doi.org/10.1109/tste.2024.3519432.
[12] D. Cazzaro, D. Koza, D. Pisinger, Combined layout and cable optimization of offshore wind farms, Eur. J. Oper. Res. 311 (1) (2023) 301–315, https://doi.org/10.1016/j.ejor.2023.04.046.
[13] X. Ding, Y. Du, X. Shen, et al., Reliability-Based planning of cable layout for offshore wind farm electrical collector System considering post-fault network reconfiguration, IEEE Trans. Sustain. Energy 16 (1) (2025) 419–433, https://doi.org/10.1109/tste.2024.3462476.
[14] J. He, M. Ge, S. Zarkovic, et al., A novel integrated optimization method of micrositing and cable routing for offshore wind farms, Energy 306 (2024) 13, https://doi.org/10.1016/j.energy.2024.132443.
[15] T. Zuo, Y. Zhang, K. Meng, et al., A two-layer hybrid optimization approach for large-scale offshore wind farm collector System planning, IEEE Trans. Ind. Inf. 17 (11) (2021) 7433–7444, https://doi.org/10.1109/tii.2021.3056428.
[16] L. Wang, J. Wu, T. Wang, et al., An optimization method based on random fork tree coding for the electrical networks of offshore wind farms, Renew. Energy 147 (2020) 1340–1351, https://doi.org/10.1016/j.renene.2019.09.100.

[17] D. Cazzaro, D. Pisinger, Balanced cable routing for offshore wind farms with obstacles, Networks 80 (4) (2022) 386–406, https://doi.org/10.1002/net.22100.
[18] R. Chen, Z. Zhang, J. Hu, et al., Grouping-based optimal design of collector system topology for a large-scale offshore wind farm by improved simulated annealing, Protection and Control of Modern Power Systems 9 (1) (2024) 94–111, https://doi.org/10.23919/pcmp.2023.000151.
[19] T. Zuo, Y. Zhang, K. Meng, et al., Collector system topology design for offshore wind farm's repowering and expansion, IEEE Trans. Sustain. Energy 12 (2) (2021) 847–859, https://doi.org/10.1109/tste.2020.3022508.
[20] S. Tao, Q. Xu, A. Feijoo, et al., Joint optimization of wind turbine micrositing and cabling in an offshore wind farm, IEEE Trans. Smart Grid 12 (1) (2021) 834–844, https://doi.org/10.1109/tsg.2020.3022378.
[21] S. Tao, F. Jiang, J. Yang, et al., Optimal cabling of deep-sea far-shore wind farm considering complex seabed and restricted zones, IEEE Trans. Ind. Inf. 21 (7) (2025) 5557–5568, https://doi.org/10.1109/tii.2025.3556038.
[22] T. Zuo, Y. Zhang, L. Xiong, et al., Complete joint-optimization for offshore wind farm planning, Int. J. Electr. Power Energy Syst. 157 (2024) 11, https://doi.org/10.1016/j.ijepes.2024.109832.
[23] M. Rentschler, F. Adam, P. Chainho, Design optimization of dynamic inter-array cable systems for floating offshore wind turbines, Renew. Sustain. Energy Rev. 111 (2019) 622–635, https://doi.org/10.1016/j.rser.2019.05.024.
[24] D. Beier, M. Ong, M. Janocha, et al., Application of suspended inter-array power cables in floating offshore wind farms, Appl. Ocean Res. 147 (2024) 17, https://doi.org/10.1016/j.apor.2024.103991.
[25] M. Lerch, M. De-Prada-Gil, C. Molins, Collection grid optimization of a floating offshore wind farm using particle swarm theory, 16th Deep Sea Offshore Wind R and D Conference (EERA DeepWind) 1356 (2019), https://doi.org/10.1088/1742-6596/1356/1/012012.
[26] M. Lerch, M. De-Prada-Gil, C. Molins, A metaheuristic optimization model for the inter-array layout planning of floating offshore wind farms, Int. J. Electr. Power Energy Syst. 131 (2021) 12, https://doi.org/10.1016/j.ijepes.2021.107128.
[27] A.I. Hietanen, T.H. Snedker, K. Dykes, et al., A novel techno-economical layout optimization tool for floating wind farm design, Wind Energy Science 9 (2) (2024) 417–438, https://doi.org/10.5194/wes-9-417-2024.
[28] D. Song, J. Yan, Y. Gao, et al., Optimization of floating wind farm power collection system using a novel two-layer hybrid method, Appl. Energy 348 (2023) 17, https://doi.org/10.1016/j.apenergy.2023.121546.
[29] E. Faraggiana, A. Ghigo, M. Sirigu, et al., Optimal floating offshore wind farms for Mediterranean islands, Renew. Energy 221 (2024) 16, https://doi.org/10.1016/j.renene.2023.119785.
[30] M. Nadimi-Shahraki, H. Zamani, Z. Varzaneh, et al., A systematic review of the whale optimization algorithm: theoretical foundation, improvements, and hybridizations, Arch. Comput. Methods Eng. 30 (7) (2023) 4113–4159, https://doi.org/10.1007/s11831-023-09928-7.
[31] H. Mohammed, S. Umar, T. Rashid, A Systematic and Meta-Analysis Survey of Whale optimization Algorithm, Comput. Intell. Neurosci. 2019 (2019) 25, https://doi.org/10.1155/2019/8718571.
[32] Qualification of innovative floating substructures for 10MW wind turbines and water depths greater than 50m. [online]. Available: https://cordis.europa.eu/project/id/640741.
[33] J. Pérez-Rúa, R. Lund, D. Verelst, et al., Exact optimization of inter-array dynamic cable networks for floating Offshore Wind farms, Renew. Energy 237 (2024) 12, https://doi.org/10.1016/j.renene.2024.121647.